Interaction of Atomically Precise Thiolated Copper Nanoclusters with Proteins: A Comparative Study

Vinitha Packirisamy and Prabhu Pandurangan*

ACCESS | 📊 Metrics & More | 📖 Article Recommendations | 🆂🅸 Supporting Information

ABSTRACT: A facile synthesis of glutathione-stabilized copper nanoclusters (CuNCs) is carried out in H_2O/ tetrahydrofuran medium. The photophysical and morphological studies performed with as-synthesized CuNCs revealed the formation of green-emissive, stable, and smaller nanoclusters. The precise composition of these as-synthesized CuNCs was predicted with the aid of electrospray ionization mass spectrometry analysis as $Cu_{12}(SG)_9$. Furthermore, the systematic studies of the interaction of synthesized CuNCs with three plasmatic proteins, namely, bovine serum albumin (BSA), lysozyme (Lys), and hemoglobin (Hb) have been performed by using a series of spectroscopic studies. The conformational changes in these proteins upon interacting with CuNCs and their binding stoichiometries have been investigated from the combination of UV−visible and steady-state fluorescence measurements. The changes in the microenvironment of proteins caused by CuNCs were investigated by circular dichroism spectroscopy. Among these three proteins, BSA and Lys had a minor effect on the luminescence of CuNCs, which makes them suitable candidates for biological applications. There are no drastic changes in the microenvironment of NCs as well as proteins because of the possibilities of weak electrostatic and H-bonding interactions of CuNCs with BSA and Lys. The feasibility of strong metallophic interaction between the Fe^{2+} present in the heme group of Hb and Cu(I) or -S atoms present in the CuNCs brings considerable changes in the photophysical activity of CuNCs and their interactions with Hb. The functional groups on NCs as well as active amino acid residues present in proteins play a crucial role in determining their interactions. This work shed a piece of knowledge on designing NCs for specific biological applications.
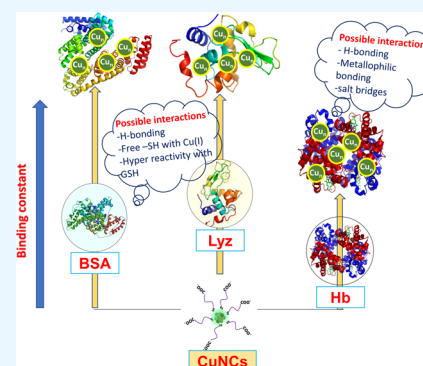
1. INTRODUCTION

Atomically precise nanoclusters with a core dimension of less than 3 nm occupy a gap between bulk atoms and nanoparticles and possess superior optical characteristics.[1] Thus the fascinating properties of metal nanoclusters (MNCs) render them applicable in sensor, catalyst, medicine, and optoelectronics fields.[1−3] The choice of ligands for stabilizing the surface of the nanocluster core regulates the nuclearity of atoms, size, structural conformation, and stability of nanoclusters.[4−6] The factors such as the choice of metals, ligands, reducing agents, and chemical environments (solvent, pH, temperature, pressure, coordinating ions) govern the composition of atoms and ligands in nanoclusters and their atomic arrangement in the core and shell, which determines their physical−chemical properties such as photoluminescence (PL), circularly polarized luminescence, magnetism, chirality, electrochemistry, and catalysis.[7−12] Because of the quantum confinement effect, lower toxicity, biocompatibility, and other peculiar characteristics of nanoclusters are widely used in biomedical fields for drug delivery, bioimaging, biomolecule sensing, cell labeling, and so on.[13−16] The extensive studies were carried out in gold nanoclusters to understand their properties that help in designing the nanoclusters with precise composition for specific applications. The extraordinary stability in aqueous medium and in atmospheric conditions

and biocompatibility nature of gold nanoclusters afford for biological applications.[17−19] The weaker stability of silver and copper nanoclusters hinders their utilization in a variety of fields. In general, the synthesis of monodisperse NCs involves two processes, that is, reduction assisted the growth of polydisperse NCs and etching mediated size focusing and most stable monodisperse nanoclusters. The series of research studies has been governed to alter the crucial factors to synthesize stable CuNCs.

On immediate exposure to biomolecules, nanoparticles readily undergo "protein-corona" formation that governs the protein−NP interactions.[20] Nanocluster surface ligand chemistry also plays a crucial role in regulating the formation of protein-corona and the interactions between them. There are plenty of studies that are explored based on the protein interaction with nanoparticles and QDs, but the detailed information of their interactions and their effect has not been

investigated.[21−23] Only minimal reports are available on the interactions of proteins with nanoclusters in the size range of below 5 nm. Among them, some reports failed to report the precise composition of NCs. In general, the properties of NCs altered with the precise composition.[24,25] The size of nanomaterials also affects the corona composition on particles and hence formed protein-corona complex mainly affects the shape of ultrasmall nanomaterials. This effect is absent in the case of large nanomaterials.[26,27] The comprehensive knowledge on the surface functionalities of NCs on protein−NC interactions is limited particularly for copper (Cu)-based nanoclusters. Hence, it is significant to obtain detailed studies of CuNCs with a known precise composition and their interactions with various kinds of proteins and their implications on biomedical studies.

Nienhaus's group reported the binding studies of dihydrolipoic acid-stabilized AgNCs and human serum albumin (HSA). The adsorption of HSA on the surface of NCs leads to the fluorescence enhancement of AgNCs. The AgNC-HSA conjugate can regulate the cell uptake responses.[28] Akhuli et al.[29] reported the interaction between CuNCs and bovine serum albumin (BSA). They reported that the binding of proteins on the NC surface was distinct from protein-corona formation. They employed tannic acid, chitosan, and cysteine-stabilized CuNCs for studying their interactions with BSA. The functionalities present in the various ligands of NCs have a profound effect on the overall protein−NC binding interactions. Yin et al.[30] derived the mechanism of interaction between gold nanoclusters (AuNCs) and HSA, transferrin, and γ-globulin.

Herein, we reported a systematic study on the binding interactions of glutathione (GSH)-protected fluorescent CuNCs with three different proteins, namely, BSA, lysozyme (Lys), and hemoglobin (Hb). Initially, green-emissive CuNCs were synthesized in H_2O/tetrahydrofuran (THF) medium. In this, GSH plays a role of a stabilizing as well as reducing agent. In comparison with H_2O medium, CuNCs synthesized in the mixture of H_2O and THF generate highly stable and fluorescent nanoclusters. As-synthesized green-emissive CuNCs were characterized by UV−visible absorption and fluorescence spectroscopy, thermogravimetric analysis (TGA), X-ray photoelectron spectroscopy (XPS) analysis, and so on. The chemical composition of as-synthesized CuNCs was determined with the aid of electrospray ionization mass spectrometry (ESI-MS) analysis. Then, the binding interaction studies of as-synthesized CuNCs against BSA, Lys, and Hb were carried out. The investigation was done by using UV−vis absorption and fluorescence spectroscopy. The conformation changes associated with proteins upon their interaction with CuNCs were monitored by circular dichroism spectroscopy.

2. EXPERIMENTAL SECTION

2.1. Materials and Instrumentation.
Cupric acetate monohydrate (min. 99%), L- glutathione reduced (GSH, min. 99%), and sodium hydroxide (min. 98%) were purchased from SRL chemicals Pvt. Ltd. Tetrahydrofuran (THF, min. 99.5%) was purchased from SRL chemicals Pvt. Ltd. Double-distilled water (DDW) was used throughout the experiments. BSA (lyophilized powder, pH −7 ≥ 98%) and Hb from bovine blood (lyophilized powder) were purchased from Sigma-Aldrich. Lysozyme (chloride) from chicken egg white was purchased from Himedia Laboratories Pvt. Ltd. All the

purchased chemicals were used as received without any further purification.

The UV−vis absorption spectrum was recorded using a Hitachi UV spectrophotometer (UH5300) with a quartz cuvette of 1 cm path length for dilute solutions of CuNCs and protein (10^{-5}−10^{-6} M). The Fourier transform-infrared (FT-IR) spectrum was recorded using a Bruker model with ATR mode. The dynamic light scattering and zeta potential measurement was performed using a Horiba SZ-100 model. The XPS analysis was carried out using a PHI-VERSAPROBE III-XPS instrument for dried powder of CuNCs. For transmission electron microscopy (TEM) imaging, the CuNCs dissolved in H_2O were sonicated and drop-cast on a carbon grid and dried under laboratory ambiance conditions, and the imaging was performed using a Jeol/Jem 2100 electron microscope. The TGA was performed using a TG/DTA − 6300 (SII − Nanotechnology, JAPAN). The thermogram was obtained for the temperature range of room temperature to 550 °C. Mass spectrometric analysis of CuNCs was carried out with ESI negative mode by using Waters LCMS equipment.

The fluorescence studies were carried out using a Horiba-Fluoromax spectrofluorometer. A quartz cell with a pathlength of 1 cm was used, and the excitation and emission slit width is maintained at 3 and 2 nm, respectively. The quantum yield of CuNCs was evaluated by the reference method by using quinine sulfate (in 0.1 M H_2SO_4) as a standard with 54% quantum yield. For quenching studies of proteins (dissolved in PBS buffer at pH −7.4) upon gradual addition of CuNCs, the spectra were monitored in the range of 300−450 nm at a fixed excitation wavelength of 280 nm. The synchronous fluorescence spectra were recorded with a slit width of Δ15 nm and Δ60 nm for the selected excitation of tyrosine and tryptophan residues, respectively. Fluorescence life time studies were examined with a time-correlated single photon counting − Fluorocube life time system. The sample was excited using a 390 nm LED, and their corresponding emission was monitored at 470 nm. Circular dichroism spectrometry analysis was performed with a CD spectrometer- Applied Photophysics Limited, UK. The CD spectra of BSA, Lys, and Hb were recorded in the range of 400−190 nm. Quartz cells with a path length of 0.1 and 0.5 cm were used, and the scanning speed was set at 200 nm min^{-1} at 25 °C. The concentration of proteins was maintained at 5 μM. Before sample measurements, under similar experimental conditions, appropriate buffer solutions were measured as blank and subtracted from the sample spectra.

2.2. Synthesis Procedure of CuNCs.
To synthesize copper nanoclusters in the metal-to-ligand ratio of 1:3, about 0.1 mmol (∼17 mg) of cupric acetate was dissolved in 10 mL of the mixture of THF with 20 mL of double-distilled water (DDW). The solution was kept under stirring for 5 min. 0.3 mmol of GSH (∼96 mg) was added to the Cu precursor solution and stirred for 30 min. The formation of a slightly white turbid solution on the addition of GSH suggests the complexing of Cu(I) with GSH. To that, 2 mL of 1 M NaOH was added and stirred for 30 min. Then the solution was kept at room temperature for about 24 h for aging. After that, 2 mL of 1 M NaOH was added. Then, the color of the solution was slowly changed from blue to green to orange. Then the solution was dried using a rotary evaporator. Similar synthesis was carried out with the same composition of metal and ligand in H_2O medium without using THF resulting in dark blue

color solution as shown in Figure 1. The resulting nanocluster sample was used for further characterization and studies.
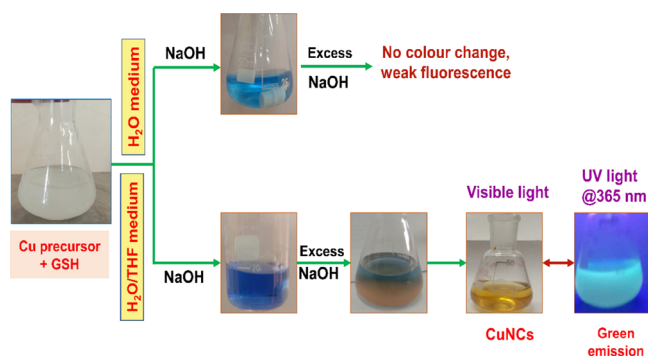
Figure 1. Schematic representation of the synthesis of CuNCs in H_2O and a mixture of H_2O/THF medium. The CuNCs synthesized in H_2O/THF medium show bright green emission under UV light at 365 nm wavelength.

3. RESULTS AND DISCUSSION

3.1. Morphological and Physicochemical Characteristics of CuNCs. In the synthesis of GSH-stabilized CuNCs, GSH served both as a stabilizing and reducing agent. In the initial stages, the complex was formed between Cu^{2+} and GSH. The addition of an excess NaOH facilitates the formation of nanoclusters by enhancing the reducing ability of the −SH group in GSH. The half-cell potential of GSH/GSSG is −0.262 V ($E°_{GSH/GSSG}$), which is highly sufficient to reduce the ionic copper into metallic copper.[31] TEM images of CuNCs synthesized in H_2O/THF medium (shown in Figure 2a) reveal that the particles are spherical and form in the size

ranges of 0.8−2.2 nm with an average size of 1.31 nm, which falls in the size ranges of atomically precise NCs.

UV−visible spectroscopy is widely utilized as an essential tool to distinguish the nanoparticle and nanocluster formation. Even the size and precise composition of nanoclusters were determined by comparing the resultant spectrum pattern with the reported materials. Because of the quantum confinement effect, the continuum band of nanoparticles breaks into discrete energy levels when approaching a smaller size. Hence, multiple absorption patterns emerged for nanoclusters. In addition to the core size of nanoclusters, the characteristics of ligands also influence the absorption pattern. The absorption spectrum of CuNCs synthesized in H_2O and H_2O/THF medium is shown in Figure 2b. The as-synthesized CuNCs in H_2O/THF medium exhibit a featureless spectrum. Two minor humps were observed at 295 and 364 nm. There are no prominent peaks seen in lower energy regions. The absence of THF during the synthesis of CuNCs promotes the nucleation of particles that produces particles in nanometer ranges. In general, the plasmon peak of copper nanoparticles was obtained at 650 nm. The existence of a broad peak at 619 nm and a minor hump at 364 nm denotes the possibility of smaller clusters. Copper nanoclusters do not possess multiple bands in the UV−vis absorption spectrum particularly in the visible region as observed for gold nanoclusters. CuNCs often have optical spectra that exhibit a steady exponential increase in absorbance at low energy and a number of bands and transitions at higher energies that are mostly regulated by the protective ligand. The absorption band or shoulder peaks observed in the region of 250−290 nm predominantly arise from the intraligand n−π* transition. The band found in the region of 300−500 nm represents the ligand-to-metal charge transfer. In CuNCs, the electronic transition is possible
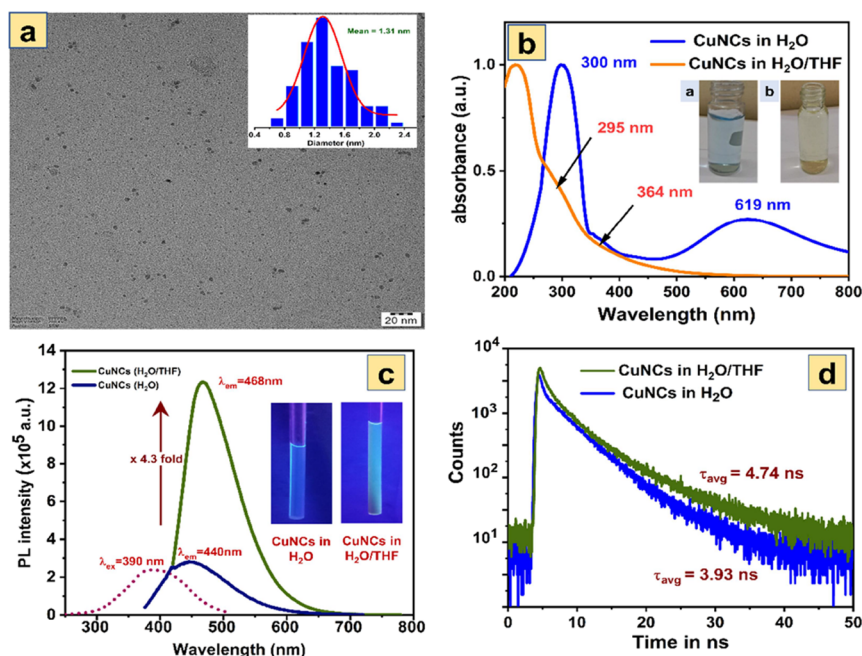
Figure 2. (a) HR-TEM image of GS-CuNCs synthesized in H_2O/THF medium. The inset shows the particle size range of 0.8−2.2 nm. (b) UV−vis absorption spectrum of GS-CuNCs synthesized in H_2O and H_2O/THF medium, (c) PL spectrum of GS-CuNCs synthesized in H_2O and H_2O/THF medium recorded at an excitation wavelength of 390 nm, and (d) time decay studies of GS-CuNCs synthesized in H_2O and H_2O/THF medium.
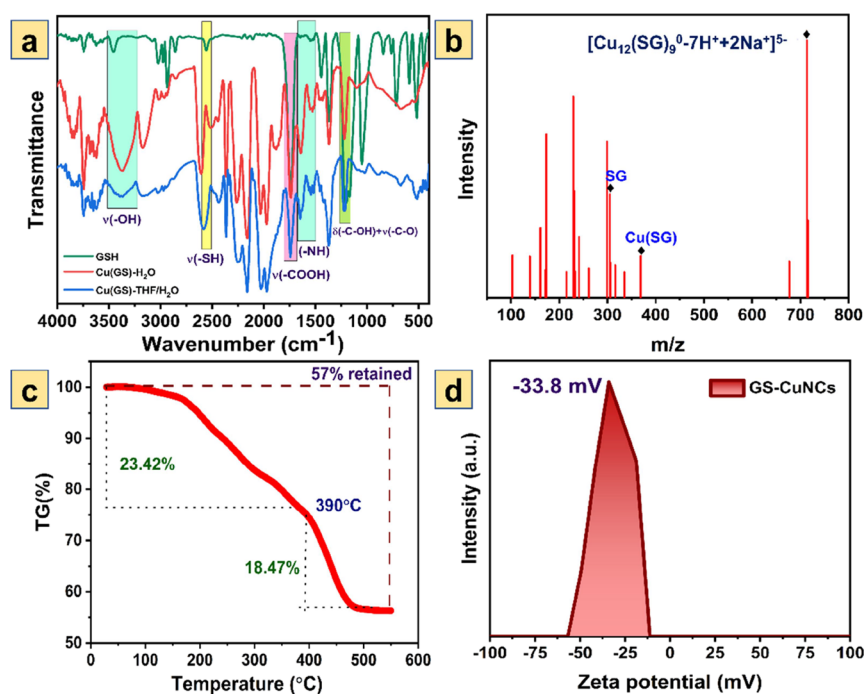
Figure 3. (a) FT-IR spectrum of GSH and GS-CuNCs synthesized in H_2O and H_2O/THF medium. (b) ESI-MS spectrum of GS-CuNCs, (c) TGA of CuNCs monitored in the temperature range of 25−550 °C, and (d) surface charge analysis of GS-CuNCs in H_2O by zeta potential analysis.

between filled Cu d-orbitals of S p-orbitals (HOMO) and empty p-orbitals of Cu atoms (LUMO).

The PL spectrum of CuNCs synthesized in H_2O and H_2O/THF medium is shown in Figure 2c. For blue-colored CuNCs, blue emission has occurred at 440 nm at an excitation wavelength of 390 nm. The yellow-colored CuNCs synthesized in H_2O/THF medium exhibit strong green emission. The PL spectrum of yellow-colored CuNCs is centered at 468 nm when excited at 390 nm. The yellow-colored solution shows bright green emission when illuminated with a 365 nm UV source. The Stokes shift is found to be 78 nm. While compared with blue-emitting CuNCs, green-emitting CuNCs have 4.3-fold higher incremental emission. The quantum yield of these blue- and green-emissive Cu nanoclusters was calculated to be 0.8 and 3.61% by using quinine sulfate in 0.1 M H_2SO_4 as a standard. The emission range of green-emitting CuNCs was monitored at different excitation wavelengths from 380 to 530 nm (shown in Figure S1), and the emission will occur in the range of 450 to 550 nm. The stability of as-synthesized CuNCs was determined by monitoring their fluorescence intensity at regular intervals of days. It was observed that the green-emitting CuNCs retained their stability for more than a month. A negligible decrease in PL intensity was observed after 6 months. In contrast to green-emissive CuNCs, the blue-emissive CuNCs lost their stability within 10 days, and the luminescence of these nanoclusters completely diminishes. This result confirms the ultrastability and highly monodisperse nature of green-emitting CuNCs. Basu et al.[32] reported the bulk-scale synthesis of cysteine-stabilized red emitting CuNCs, which lost its stability within 20 days. Even the mixture of solvents in synthesis could not retain stability, which easily undergoes degradation due to oxidation. They revealed the considerable effect of solvent in determining the stability and formation of CuNCs. The average lifetime measurement of CuNCs synthesized in H_2O and H_2O/THF medium is shown in Figure 2d. The average excited state lifetime of 3.93 ns was

recorded for freshly prepared blue-emissive CuNCs at an excitation and emission wavelength of 390 and 440 nm respectively. For green-emissive CuNCs, the average lifetime was calculated to be 4.74 ns recorded at an excitation and emission wavelength of 390 and 470 nm, respectively. The possibility of longer extent radiative relaxation is responsive to fluorescence enhancement in green-emissive nanoclusters.

FT-IR spectroscopy reveals information of functional group presence, nature of ligand interaction with metal atoms, and impact of solvent in nanoclusters. The IR spectrum of GSH and Cu-GS synthesized in H_2O/THF and H_2O is shown in Figure 3a. The disappearance of S−H vibration of GSH in CuNCs at 2559 cm^{-1} signifies the stabilization of GS over the surface of the Cu atom core in CuNCs via Cu−S bonding. The characteristic stretching frequency of −COOH and −NH$_2$ was observed at 1735 and 1650−1527 cm^{-1}. The peak at 1215 cm^{-1} was associated with the stretching and bending vibration of the carbonyl group present in the ligand. The peak at 3460 cm^{-1} represents the −OH stretching frequency. The shift in the −OH stretching frequency arises from the intra or intermolecular H-bonding. Additionally, the peak broadening was observed at the peak associated with the carbonyl group, due to the changes in a chemical environment associated with a specific element that bonded with other groups.[33] The introduction of a polar aprotic solvent, that is, THF as a poor solvent during the synthesis of CuNCs involves in size-control of NCs and regulation of the ligand over the Cu core. The effect of polar protic and aprotic solvents on the physicochemical properties of thiophenol-stabilized cobalt nanoclusters was investigated by our group.[33] The changes associated with the H-bonding formation and etching of weak ligands over nanoclusters bring prominent changes in their luminescence behavior. The possibility of intermolecular H-bonding while synthesis CuNCs in water brought the molecules together to form larger aggregates, which was evidenced by −OH peak broadening. The peak broadening
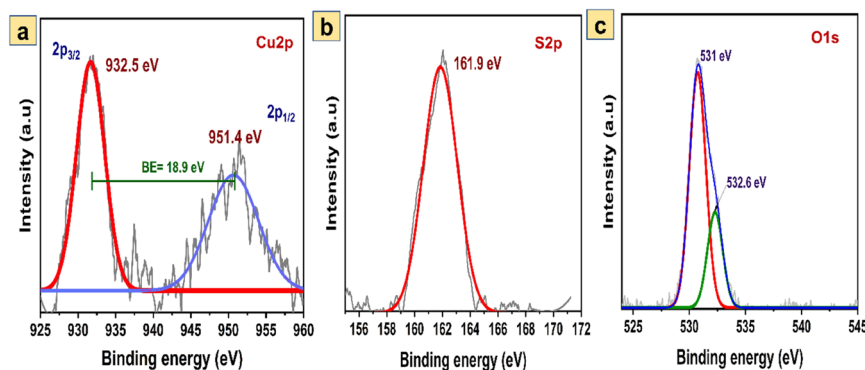
Figure 4. X-ray photoelectron spectra of CuNCs (a) Cu 2p, (b) S 2p, and (c) O 1s.

and lower frequency shifting associated with the carbonyl group of CuNCs synthesized in THF/H_2O signify the presence of intramolecular H-bonding. In comparison with intramolecular bonding, intermolecular H-bonding does not possess stability, which could break easily during environmental changes.

The exact molecular composition of green-emissive CuNCs was predicted by ESI-MS in negative-ion mode (illustrated in Figure 3b).The more intense (m/z) peak at 713.4 Da was assigned as $[Cu_{12}(SG)_9-7H^+ + 2Na^+]^{5-}$. The remaining peaks arise because of the fragmentation of $Cu_{12}(SG)_9$ NCs. TGA as illustrated in Figure 3c was used to investigate the robustness of GS-stabilized CuNCs. The two-step decomposition observed in the TG profile may have resulted from the removal of weakly and strongly adsorbed ligands from the surface of NCs. A weight loss of 23.42% was observed in the range of 25 to 390 °C, which signifies the detachment of weakly adsorbed ligands and 18.47% of weight loss observed at the range of 390 to 500 °C, because of the removal of strongly adsorbed ligands by breaking the covalent linkage between metal atoms and S atoms present in ligand. Beyond 500 °C, the decay curve in TGA gets saturated indicating the complete removal of GS from NCs, at the end approximately ∼57% of the weight was retained. The TGA results validate the formation of CuNCs with a metal-to-ligand ratio of 1:0.75, which was corroborated by ESI-MS analysis. The surface charge over the CuNCs was analyzed with zeta potential measurements as shown in Figure 3d. The zeta potential of −33.8 mV observed for GS-stabilized green-emissive CuNCs evidenced their colloidal stability in an aqueous medium and the negative charge over their surface. The negative charge that arises from the deprotonation of GS ligand generates carboxylate ions on excessive addition of NaOH for stable NC formation.

The oxidation states of Cu, S, and O in CuNCs synthesized in THF/H_2O were characterized using XPS measurements. The survey spectrum shows the binding energy signals of various chemical entities present in CuNCs. As illustrated in Figure 4a, two distinct peaks were found at 932.5 and 951.4 eV corresponding to $2p_{3/2}$ and $2p_{1/2}$, respectively. The binding energy between these peaks was evaluated to be 18.9 eV. The absence of a satellite peak around 938−942 eV reveals the absence of Cu(II) in CuNCs. The lower difference of 0.3 eV in the binding energies of Cu(I) and Cu(O) hinders from further deconvolution. The peak observed at 161.9 eV was assigned as S $2p_{3/2}$, confirming the bonding of Cu(I)−S in CuNCs through covalent bonding (shown in Figure 4b). The XPS spectrum of O 1s is shown in Figure 4c. The spectrum

obtained for CuNCs was deconvoluted into two peaks at 531 and 532.6 eV representing C−O and C=O bonding present in GS ligand stabilizing over the CuNC core. The metal oxide peak generally appeared at 529−530 eV, and the absence of such a peak confirms the bonding of Cu with sulfur, not with oxygen. The proportion of metal to ligand in the formation of CuNCs was evaluated to be 1:3 from the atomic weight percentage obtained in XPS. Overall XPS and IR results suggest that core Cu atom stabilization occurs via bonds with S atoms rather than the O atom found in the GSH ligand.

3.2. Probing Protein−Copper Nanocluster Interactions through UV−vis Absorption and Steady-State Fluorescence Measurements. The specific molecular interaction between CuNCs and three different proteins, namely, BSA, Lys, and Hb was investigated by monitoring the absorption spectrum on gradual addition of CuNCs to proteins. The absorption peak observed at 278 nm solely corresponds to BSA (shown in Figure S2). The absorbance of that peak gradually increases by increasing the concentration of nanoclusters. The absence of peaks shift on nanoclusters addition signifies the feasibility of the ground-state complex between protein and [CuNCs]. The peak corresponding to Lys that appeared at 281 nm blue shifted to 268 nm on gradual addition of nanoclusters. The addition of nanoclusters into proteins forms the complex. The three major amino acids, namely, phenylalanine, tyrosine, and tryptophan are the reasons for an intrinsic fluorescence of BSA proteins. While compared with the fluorescence of tryptophan and tyrosine, phenylalanine has negligible fluorescence. Hence that is not considered in this study. In the case of Lys, the gradual addition of CuNCs induces the blue shift at peak maxima. The characteristic peaks of Hb have been observed at around 277 and 400 nm. The peak at 277 nm shifts to 268 nm upon increasing the concentration of CuNCs. For Hb, the minimal 10 nm peak shift was observed on increasing the concentration of CuNCs. The peak at 277 nm is attributed to the phenyl group of tyrosine and tryptophan residues, and the peak at 406 nm represents that the Soret band arises from $\pi-\pi^*$ transition of the heme group. The folded or native structure of Hb was confirmed from the existence of the Soret band at 406 nm. The changes in the Soret band are accompanied by the reduction in the α-helix content, during interactions with external factors. The linear decreases in absorbance without any peak shifts observed in Soret band represent the weak H-bonding, electrostatic, or hydrophobic interactions between Hb and CuNCs.[34] The effective interaction of CuNCs with proteins is also detected by fluorescence quenching measurements (shown in Figure 5a−c). The fluorescence emission spectra
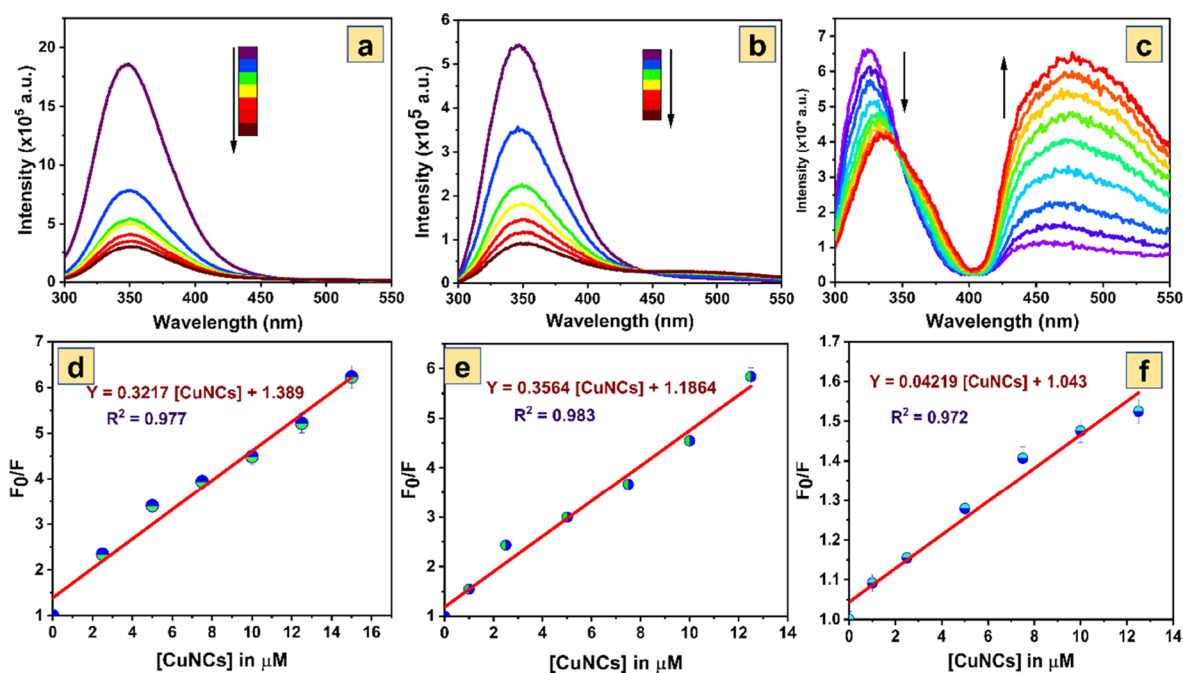
Figure 5. Fluorescence quenching spectra of (a) BSA, (b) Lys, and (c) Hb on increasing the concentration of [CuNCs]. Stern−Volmer plots of the fluorescence quenching (d) BSA, (e) Lys, and (f) Hb by CuNCs.
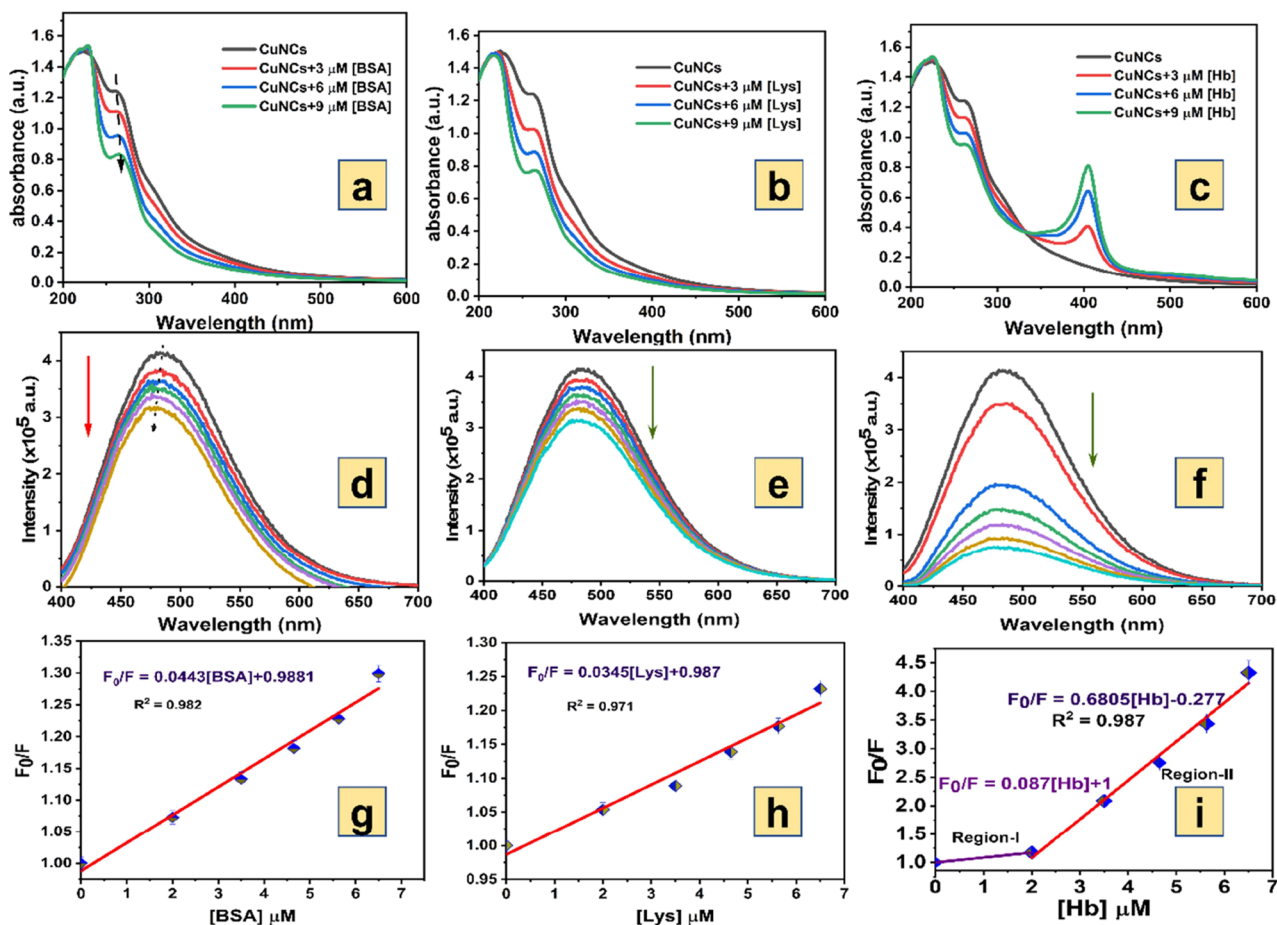
Figure 6. UV−vis absorption spectrum of CuNCs on increasing concentration of (a) BSA, (b) Lys, and (c) Hb. Fluorescence quenching spectra of CuNCs upon gradual addition of (d) BSA, (e) Lys, and (f) Hb. (g−i) Shows the Stern−Volmer plots of the fluorescence quenching of CuNCs by BSA, Lys, and Hb, respectively.
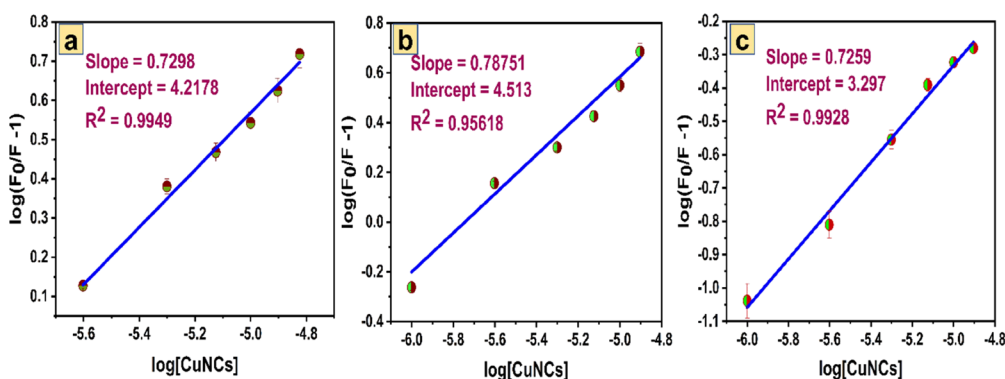
Figure 7. −B−H double-logarithmic plot for the binding of CuNCs with (a) BSA, (b) Lys, and (c) Hb respectively.

of pure proteins in the presence and absence of NCs were measured. BSA shows a strong emission band around 347 nm at an excitation wavelength of 280 nm. Upon gradual addition of CuNCs, the fluorescence intensity decreases steeply and beyond saturation at some point, the intensity decreases will be low. The fluorescence quenching of protein on the addition of the CuNCs was fitted in the Stern−Volmer equation stated as follows:

$$F_0/F = 1 + K_{SV}[Q]$$

where F_0 and F are the fluorescence intensity of BSA observed at 347 nm in the absence and presence of [CuNCs], respectively. K_{SV} is the Stern−Volmer quenching constant, which can be calculated from the slope derived by the plot of [CuNCs] vs F_0/F. [Q] is the concentration of the quencher; in this case, it is CuNCs. For Hb, compared with the fluorescence that arises from protein which appeared as a peak at 340 nm, the fluorescence peak of the heme group at around 480 nm experiences the fluorescence enhancement. This may arise from the active interaction of CuNCs toward the iron(Fe)-containing heme group present in the Hb. The fluorescence quenching rate of BSA, Lys, and Hb differs on the addition of CuNCs. This is due to the active groups present in the proteins. The Stern−Volmer quenching constant (K_{SV}) for BSA, Lys, and Hb by CuNCs was determined to be 0.3217, 0.3567, and 0.04219, respectively, from the Stern−Volmer plot (shown in Figure 5d−f). The higher quenching rate observed for BSA and Lys is due to the presence of sulfur atoms in protein interacting with the Cu(I) ions of CuNCs. BSA has one free thiol group along with 17 intrachain disulfide bonds. Lys contains eight cysteine residues of the protein. The higher fluorescence quenching may be the result of bonding interactions of cysteine moieties present in the protein and CuNCs. The interaction of protein with CuNCs leads to changes in the structure of proteins. Such changes show a profound effect on their functions. Hence, it is vital to investigate the structural changes caused by CuNCs. Most probably, the proteins also bring the marked effect in the structure of CuNCs. The negligible changes can be seen in the spectral pattern of CuNCs on increasing concentration of BSA, Lys, and Hb (shown in Figure 6a−c). The weaker interaction of cysteine residues present in the protein and CuNCs may be the reason for the null changes in the spectral pattern of CuNCs. When the GS-CuNCs was treated with an increasing concentration of BSA, Lys, and Hb, the fluorescence of CuNCs at 475 nm was gradually quenched (shown in Figure 6d−f), and their corresponding calibration plot is shown in Figure

6g−i. The results obtained were contrary to the incremental emission of CuNCs on the gradual addition of HSA reported by Kumar Das et al.[35] They stated that the addition of HSA generates a hydrophobic environment that results in a fluorescence enhancement because of the formation of protein-corona-like assemblies. This information reveals that the interaction between GS-CuNCs and protein is not through protein-corona formation. While comparing the quantity of fluorescence quenching, Hb had more effect on the photophysical properties of CuNCs, whereas BSA and Lys had minimal influence on the fluorescence properties of CuNCs. The stoichiometry of binding of proteins with NCs can be deduced from the modified Benesi−Hildebrand (B−H) double-reciprocal plot. The complexation stoichiometry of protein and NCs was determined from the following equation:

$$\frac{1}{F - F_0} = \frac{1}{F_m - F_0} + \frac{1}{(F_m - F_0)K[BSA]}$$

where F and F_m are the fluorescence intensity of CuNCs with addition of protein and maximum protein concentration, respectively. F_0 is the fluorescence intensity in the absence of protein, K is the equilibrium constant. The B−H plots for CuNCs 1:1 complexation with BSA, Lys, and Hb are shown in Figure S3a−c. A good linear correlation obtained in the plot of 1/[protein] vs $1/F - F_0$ evidenced the binding of BSA and Lys with CuNCs in 1:1 stoichiometric ratio. In the case of Hb, some points that deviate from the linearity at initial additions (shown in Figure 6i) suggest that the stoichiometry complexation of Hb with CuNCs will be multiple. These studies imply that the interaction of proteins and NCs has not been led by the formation of protein-corona like assemblies. The binding interactions of proteins with CuNCs induces the aggregation of proteins over the NCs and thereby increases the hydrodynamic size of NCs (shown in Figure S4a). The hydrodynamic size of CuNCs was found to be in the range of 100−130 nm. Upon introduction of BSA, Lys, and Hb, the hydrodynamic sizes increase to 5200−8400 nm, 3800−8400 nm, and 490−1200 nm, respectively. The aggregation of proteins and CuNCs promotes the size increment. The feasibility of electrostatic interactions between protein and CuNCs was revealed from the decrease in the zeta potential as well as shifted toward neutralizing the charge of CuNCs upon addition of BSA, Lys, and Hb (shown in Figure S4b).

The double-logarithmic plot predicts the binding interaction between protein and nanoclusters that was determined from the fluorescence quenching of proteins on the gradual addition of CuNCs. Double-logarithmic curves of BSA, Lys, and Hb on

CuNC addition are shown in Figure 7a−c, respectively. The binding constant obtained for BSA, Lys, and Hb is tabulated in Table 1, and these obtained results are compared with the

Table 1. Stern−Volmer Quenching Constant, Quenching Rate Constant, Associative Binding Constant, and Number of Binding Sites for the Interaction of CuNCs with BSA, Lys, and Hb

protein	$K_{sv} \times 10^5$ M^{-1}	$K_q \times 10^{12}$ M^{-1} S^{-1}	$K_b \times 10^5$ M^{-1}	N
BSA	3.217 ± 0.22	3.217 ± 0.22	6.97 ± 0.02	0.73
Lys	3.564 ± 0.21	3.564 ± 0.21	6.45 ± 0.04	0.79
Hb	0.422 ± 0.03	0.422 ± 0.03	1.32 ± 0.10	0.73

reported MNCs/MNP and their interactions with proteins (shown in Table S1). It is observed that the magnitude of K_b is 10^4, during interaction of large metal nanoparticles with proteins. The binding interactions of proteins will be stronger for smaller metal nanoclusters with the magnitude of 10^5, and their values also differ based on the type of MNCs and proteins. The resultant data substantiate the one mode of binding for CuNCs with BSA and Lys irrespective of the functional groups present in the proteins.

3.3. Conformational Changes Resulting from CuNCs−Protein Interactions.

The conformational changes that occurred in the protein molecules are commonly examined with the aid of circular dichroism spectroscopic measurements, which reveal information on the interaction of various chemical entities on the optically active protein or peptide molecules.[36] Wang et al. reported the conformational changes in the secondary structure of BSA on the AuNP surface. The interaction of Au atoms with sulfur in proteins promotes the transformation of disulfide bonds into S−Au coordination, thereby decreasing the α-helices and increasing the β-sheet structures.[37] On the addition of CuNCs (5 μM), the α-helix content of BSA decreases to 26.13% from 30.82%. The α-helix content of Lys and Hb also decreases upon addition of CuNCs. The changes associated with the CD spectrum of BSA, Lys, and Hb upon addition of CuNCs are shown in Figure 8a−c and Table S2, respectively. There were no predominant changes observed in the spectrum of BSA and Lys upon addition of CuNCs. As discussed earlier, this may be due to the weaker interaction of proteins with CuNCs that brings minor changes in the environment around proteins and thereby induces the decreases in the α-helical structure of protein with increasing β-sheet structures. The profound changes observed for Hb at around 220 nm arise from the
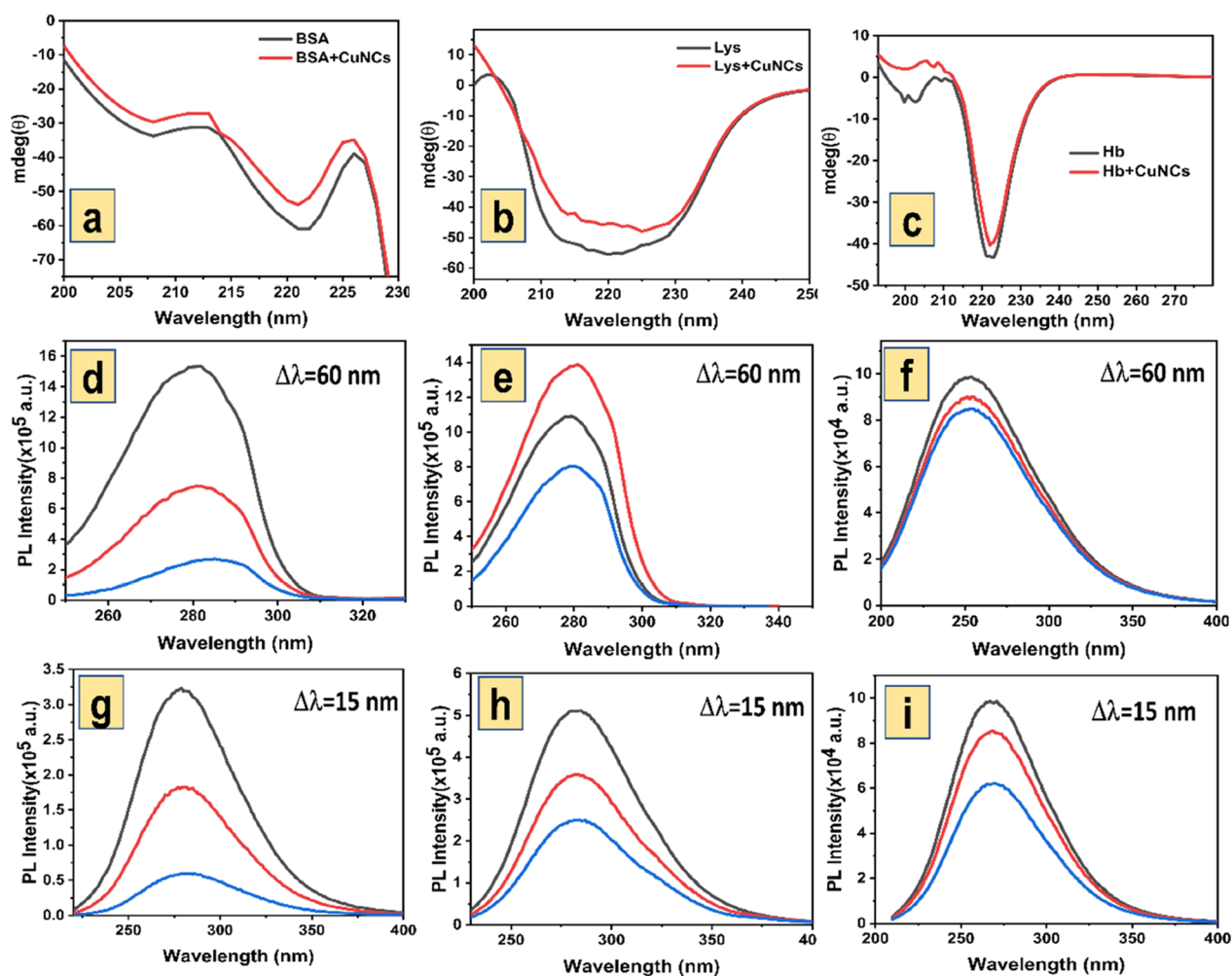
Figure 8. Far-UV circular dichroism spectra of (a) BSA, (b) Lys, and (c) Hb in the presence (red line) and absence (black line) of CuNCs. Synchronous fluorescence spectra of (d, g) BSA, (e, h) Lys, and (f, i) Hb with gradual addition of CuNCs (black line −0 μM, red line −3 μM, blue line −7 μM of CuNCs). Spectrum monitored with an offset wavelength of 60 and 15 nm.

possible interactions of the Fe group present in the heme group of Hb and CuNCs brought microenvironmental changes around the amino acid residues of proteins were monitored by observing the spectral pattern in the range of 260−350 nm, both in the presence and the absence of CuNCs (shown in Figure S5). No prominent changes observed in the spectrum of BSA, Lys, and Hb suggest that the tertiary of structure of proteins remains unaltered during interaction with CuNCs.

Synchronous fluorescence measurements have been performed to investigate the conformational induced in protein molecules by CuNCs by interacting with it (shown in Figure 8d−i). The changes associated with the microenvironment of fluorophores moieties present in protein causes the shift in maximum emission wavelength. The characteristic information of tyrosine and tryptophan residues present in protein was monitored by fixing offset wavelength of ($\Delta\lambda$) of 15 and 60 nm. Upon gradual addition of CuNCs, the increasing concentration of nanoclusters quenches the synchronous fluorescence of BSA, Lys, and Hb. The quenching of fluorescence reveals the interaction of these nanoclusters through tryptophan and tyrosine residues. No changes observed in the peak shift suggest that the microenvironment of tryptophan and tyrosine remains unaltered.[38]

4. CONCLUSIONS

In this work, we report the facile synthesis of stable CuNCs in H_2O/THF medium. The CuNCs synthesized in H_2O lost their stability and fluorescence ability on reacting with atmospheric conditions. The as-synthesized stable CuNCs show a green fluorescence emission at 470 nm at an excitation wavelength of 390 nm. The quantum yield of these CuNCs is calculated to be 3.61% by using quinine sulfate as a standard. The green emission of these CuNCs was long-lasting for more than 6 months, which reveals their stability nature. The precise composition of these clusters was predicted as $Cu_{12}(SG)_9$ by negative-mode ESI-MS measurement. The metal-to-ligand ratio and thermal robustness of CuNCs were tested by adopting TGA. The surface charge over the CuNCs was determined by zeta potential analysis as −33.8 mV. Furthermore, the binding interaction of these nanoclusters with proteins like BSA, Lys, and Hb was studied for their future implications in the biomedical field as a therapeutic agent for drug delivery, biolabeling, and bioimaging applications to diagnose and treat diseases. From the series of UV−vis absorption and fluorescence studies, the nature of binding between CuNCs and proteins was investigated. The fluorescence quenching of CuNCs by BSA and Lys is due to the weaker interaction of cysteine residues in protein and Cu(I) ions present in CuNCs. The profound quenching of CuNCs by Hb may be caused by the interaction of CuNCs predominantly with the heme group rather than macromolecules of Hb. The binding stoichiometry of CuNCs with protein was found to be 1:1, which was deducted by the B−H equation. The conformational changes determined from circular dichroism spectroscopy reveal the structural changes in altering the content α-helix and β-sheet structures. The outcome of this study is expected to encourage fabrication of various metal nanoclusters according to specific biomedical applications.

■ ASSOCIATED CONTENT

Ⓢ Supporting Information

The Supporting Information is available free of charge at https://pubs.acs.org/doi/10.1021/acsomega.2c06011.

> Binding constant and α-helix content calculation, excitation-dependent emission spectrum of CuNCs, absorption spectrum of BSA, Lys, and Hb upon gradual addition of CuNCs, Benesi−Hildebrand double-reciprocal plot of CuNCs with BSA, Lys, and Hb, and near UV-CD spectrum of BSA, Lys, and Hb in the presence and absence of CuNCs (PDF)

■ AUTHOR INFORMATION

Corresponding Author

Prabhu Pandurangan − *Department of Physical Chemistry, School of Chemical Science, University of Madras, Chennai, Tamilnadu 600 025, India;* ⓞ orcid.org/0000-0002-1137-2753; Email: pprabhumu@gmail.com

Author

Vinitha Packirisamy − *Department of Physical Chemistry, School of Chemical Science, University of Madras, Chennai, Tamilnadu 600 025, India*

Complete contact information is available at:
https://pubs.acs.org/10.1021/acsomega.2c06011

Notes

The authors declare no competing financial interest.

■ ACKNOWLEDGMENTS

■ REFERENCES

(1) Jin, R.; Zeng, C.; Zhou, M.; Chen, Y. Atomically Precise Colloidal Metal Nanoclusters and Nanoparticles: Fundamentals and Opportunities. *Chem. Rev.* **2016**, *116*, 10346−10413.

(2) Pelayo, J. J.; Whetten, R. L.; Garzón, I. L. Geometric Quantification of Chirality in Ligand-Protected Metal Clusters. *J. Phys. Chem. C* **2015**, *119*, 28666−28678.

(3) Jin, R. Atomically Precise Metal Nanoclusters: Stable Sizes and Optical Properties. *Nanoscale* **2015**, *7*, 1549−1565.

(4) Heuer-Jungemann, A.; Feliu, N.; Bakaimi, I.; Hamaly, M.; Alkilany, A.; Chakraborty, I.; Masood, A.; Casula, M. F.; Kostopoulou, A.; Oh, E.; Susumu, K.; Stewart, M. H.; Medintz, I. L.; Stratakis, E.; Parak, W. J.; Kanaras, A. G. The Role of Ligands in the Chemical Synthesis and Applications of Inorganic Nanoparticles. *Chem. Rev.* **2019**, *119*, 4819−4880.

(5) Wan, X. K.; Wang, J. Q.; Nan, Z. A.; Wang, Q. M. Ligand Effects in Catalysis by Atomically Precise Gold Nanoclusters. *Sci. Adv.* **2017**, *3*, No. e1701823.

(6) Wu, Z.; Jin, R. On the Ligand's Role in the Fluorescence of Gold Nanoclusters. *Nano Lett.* **2010**, *10*, 2568−2573.

(7) Wu, Z.; Li, Y.; Liu, J.; Lu, Z.; Zhang, H.; Yang, B. Colloidal Self-Assembly of Catalytic Copper Nanoclusters into Ultrathin Ribbons. *Angew. Chem., Int. Ed.* **2014**, *53*, 12196−12200.

(8) Kwak, K.; Lee, D. Electrochemistry of Atomically Precise Metal Nanoclusters. *Acc. Chem. Res.* **2019**, *52*, 12−22.

(9) Zhang, J.; Li, Z.; Huang, J.; Liu, C.; Hong, F.; Zheng, K.; Li, G. Size Dependence of Gold Clusters with Precise Numbers of Atoms in Aerobic Oxidation of D-Glucose. *Nanoscale* **2017**, *9*, 16879−16886.

(10) Shen, J.; Wang, Z.; Sun, D.; Xia, C.; Yuan, S.; Sun, P.; Xin, X. PH-Responsive Nanovesicles with Enhanced Emission Co-Assembled by Ag(I) Nanoclusters and Polyethyleneimine as a Superior Sensor for Al3+. *ACS Appl. Mater. Interfaces* **2018**, *10*, 3955−3963.

(11) Green, T. D.; Yi, C.; Zeng, C.; Jin, R.; McGill, S.; Knappenberger, K. L. Temperature-Dependent Photoluminescence of Structurally-Precise Quantum-Confined Au25(SC8H9)18 and Au38(SC12H25)24 Metal Nanoparticles. *J. Phys. Chem. A* **2014**, *118*, 10611−10621.

(12) Huang, Y.; Feng, H.; Liu, W.; Zhang, S.; Tang, C.; Chen, J.; Qian, Z. Cation-Driven Luminescent Self-Assembled Dots of Copper Nanoclusters with Aggregation-Induced Emission for β-Galactosidase Activity Monitoring. *J. Mater. Chem. B* **2017**, *5*, 5120−5127.

(13) Kang, X.; Zhu, M. Tailoring the Photoluminescence of Atomically Precise Nanoclusters. *Chem. Soc. Rev.* **2019**, *48*, 2422−2457.

(14) McNamara, K.; Tofail, S. A. M. Nanoparticles in Biomedical Applications. *Adv. Phys.: X.* **2017**, *2*, 54−88.

(15) Zheng, K.; Yuan, X.; Goswami, N.; Zhang, Q.; Xie, J. Recent Advances in the Synthesis, Characterization, and Biomedical Applications of Ultrasmall Thiolated Silver Nanoclusters. *RSC Adv.* **2014**, *4*, 60581−60596.

(16) Zheng, K.; Xie, J. Engineering Ultrasmall Metal Nanoclusters as Promising Theranostic Agents. *Trends Chem.* **2020**, *2*, 665−679.

(17) Chen, P. C.; Chiang, C. K.; Chang, H. T. Synthesis of Fluorescent BSA-Au NCs for the Detection of Hg2+ Ions. *J. Nanopart. Res.* **2012**, *15*, 1−10.

(18) Tam, J. M.; Tam, J. O.; Murthy, A.; Ingram, D. R.; Ma, L. L.; Travis, K.; Johnston, K. P.; Sokolov, K. V. Controlled Assembly of Biodegradable Plasmonic Nanoclusters for Near-Infrared Imaging and Therapeutic Applications. *ACS Nano* **2010**, *4*, 2178−2184.

(19) Kuo, S. H.; Chien, C. S.; Wang, C. C.; Shih, C. J. Antibacterial Activity of Bsa-Capped Gold Nanoclusters against Methicillin-Resistant Staphylococcus Aureus (Mrsa) and Vancomycin-Intermediate Staphylococcus Aureus (VISA). *J. Nanomater.* **2019**, *2019*, No. 4101293.

(20) Durán, N.; Silveira, C. P.; Durán, M.; Martinez, D. S. T. Silver Nanoparticle Protein Corona and Toxicity: A Mini-Review. *J. Nanobiotechnol.* **2015**, *13*, 55.

(21) Wang, H.; Shang, L.; Maffre, P.; Hohmann, S.; Kirschhöfer, F.; Brenner-Weiß, G.; Nienhaus, G. U. The Nature of a Hard Protein Corona Forming on Quantum Dots Exposed to Human Blood Serum. *Small* **2016**, *12*, 5836−5844.

(22) Qu, S.; Sun, F.; Qiao, Z.; Li, J.; Shang, L. In Situ Investigation on the Protein Corona Formation of Quantum Dots by Using Fluorescence Resonance Energy Transfer. *Small* **2020**, *16*, No. 1907633.

(23) Gunawan, C.; Lim, M.; Marquis, C. P.; Amal, R. Nanoparticle-Protein Corona Complexes Govern the Biological Fates and Functions of Nanoparticles. *J. Mater. Chem. B* **2014**, *2*, 2060−2083.

(24) Yu, H.; Rao, B.; Jiang, W.; Yang, S.; Zhu, M. The photoluminescent metal nanoclusters with atomic precision. *Coord. Chem. Rev.* **2019**, *378*, 595−617.

(25) Tang, Q.; Hu, G.; Fung, V.; Jiang, D. E. Insights into Interfaces, Stability, Electronic Properties, and Catalytic Activities of Atomically Precise Metal Nanoclusters from First Principles. *Acc. Chem. Res.* **2018**, *51*, 2793−2802.

(26) Sasidharan, A.; Riviere, J. E.; Monteiro-Riviere, N. A. Gold and Silver Nanoparticle Interactions with Human Proteins: Impact and Implications in Biocorona Formation. *J. Mater. Chem. B* **2015**, *3*, 2075−2082.

(27) Zuo, G.; Kang, S. G.; Xiu, P.; Zhao, Y.; Zhou, R. Interactions between Proteins and Carbon-Based Nanoparticles: Exploring the Origin of Nanotoxicity at the Molecular Level. *Small* **2013**, *9*, 1546−1556.

(28) Shang, L.; Dörlich, R. M.; Trouillet, V.; Bruns, M.; Nienhaus, G. U. Ultrasmall Fluorescent Silver Nanoclusters: Protein Adsorption and Its Effects on Cellular Responses. *Nano Res.* **2012**, *5*, 531−542.

(29) Akhuli, A.; Chakraborty, D.; Agrawal, A. K.; Sarkar, M. Probing the Interaction of Bovine Serum Albumin with Copper Nanoclusters: Realization of Binding Pathway Different from Protein Corona. *Langmuir* **2021**, *37*, 1823−1837.

(30) Yin, M. M.; Chen, W. Q.; Lu, Y. Q.; Han, J. Y.; Liu, Y.; Jiang, F. L. A Model beyond Protein Corona: Thermodynamics and Binding Stoichiometries of the Interactions between Ultrasmall Gold Nanoclusters and Proteins. *Nanoscale* **2020**, *12*, 4573−4585.

(31) Baghdasaryan, A.; Grillo, R.; Roy Bhattacharya, S.; Sharma, M.; Reginato, E.; Theraulaz, H.; Dolamic, I.; Dadras, M.; Rudaz, S.; Varesio, E.; Burgi, T. Facile Synthesis, Size-Separation, Characterization, and Antimicrobial Properties of Thiolated Copper Clusters. *ACS Appl. Nano Mater.* **2018**, *1*, 4258−4267.

(32) Basu, K.; Paul, S.; Jana, R.; Datta, A.; Banerjee, A. Red-Emitting Copper Nanoclusters: From Bulk-Scale Synthesis to Catalytic Reduction. *ACS Sustainable Chem. Eng.* **2019**, *7*, 1998−2007.

(33) Packirisamy, V.; Subramanian, R.; Pandurangan, P. Solvent-Driven Thiol Protected Luminescent Cobalt Nanoclusters. *J. Mol. Liq.* **2022**, *354*, No. 118857.

(34) Vashishat, R.; Chabba, S.; Mahajan, R. K. Surface Active Ionic Liquid Induced Conformational Transition in Aqueous Medium of Hemoglobin. *RSC Adv.* **2017**, *7*, 13041−13052.

(35) Kumar Das, N.; Chakraborty, S.; Mukherjee, M.; Mukherjee, S. Enhanced Luminescent Properties of Photo-Stable Copper Nanoclusters through Formation of "Protein-Corona"-Like Assemblies. *ChemPhysChem* **2018**, *19*, 2218−2223.

(36) Mishra, R. K.; Ahmad, A.; Vyawahare, A.; Alam, P.; Khan, T. H.; Khan, R. Biological Effects of Formation of Protein Corona onto Nanoparticles. *Int. J. Biol. Macromol.* **2021**, *175*, 1−18.

(37) Wang, L.; Li, J.; Pan, J.; Jiang, X.; Ji, Y.; Li, Y.; Qu, Y.; Zhao, Y.; Wu, X.; Chen, C. Revealing the Binding Structure of the Protein Corona on Gold Nanorods Using Synchrotron Radiation-Based Techniques: Understanding the Reduced Damage in Cell Membranes. *J. Am. Chem. Soc.* **2013**, *135*, 17359−17368.

(38) Pavani, P.; Kumar, K.; Rani, A.; Venkatesu, P.; Lee, M. J. The Influence of Sodium Phosphate Buffer on the Stability of Various Proteins: Insights into Protein-Buffer Interactions. *J. Mol. Liq.* **2021**, *331*, No. 115753.